Structural and electronic properties
of highly doped topological insulator Bi₂Se₃ crystals

Helin Cao[*, 1, 2], **Suyang Xu**[3, 4], **Ireneusz Miotkowski**[1], **Jifa Tian**[1, 2], **Deepak Pandey**[1, 2], **M. Zahid Hasan**[3, 4], **and Yong P. Chen**[*, 1, 2, 5]

[1] Department of Physics, Purdue University, 525 Northwestern Ave., West Lafayette, IN 47907, USA
[2] Birck Nanotechnology Center, Purdue University, 1205 W. State St., West Lafayette, IN 47907, USA
[3] Joseph Henry Laboratories, Department of Physics, Princeton University, Jadwin Hall, Princeton, NJ 08544, USA
[4] Princeton Institute for Science and Technology of Materials, Princeton University, 70 Prospect Ave., Princeton, NJ 08544, USA
[5] School of Electrical and Computer Engineering, Purdue University, 465 Northwestern Ave., West Lafayette, IN 47907 USA

[*] Corresponding authors: e-mail cao2@purdue.edu, Phone: +01 765 496 3059, Fax: +01 765 494 0706;
e-mail yongchen@purdue.edu, Phone: +01 765 494 0947, Fax: +01 765 494 0706

We present a study of the structural and electronic properties of highly doped topological insulator Bi₂Se₃ single crystals synthesized by the Bridgman method. Lattice structural characterizations by X-ray diffraction, scanning tunneling microscopy, and Raman spectroscopy confirmed the high quality of the as-grown single crystals. The topological surface states in the electronic band structure were directly revealed by angle-resolved photoemission spectroscopy. Transport measurements showed that the conduction was dominated by the bulk carriers and confirmed a previously observed bulk quantum Hall effect in such highly doped Bi₂Se₃ samples. We briefly discuss several possible strategies of reducing bulk conductance.

1 Introduction The electronic properties of Bi₂Se₃, a semiconductor made of van der Waals coupled stacking "quintuple layers" (QL), were thought to be well understood since it had been studied for decades in light of its excellent thermoelectric properties. However, recently, it has been revealed that Bi₂Se₃ belongs to a new class of quantum materials: three-dimensional (3D) topological insulators (TI) [1, 2]. In a 3D TI, the bulk has a band gap (~0.3 eV for Bi₂Se₃), and the surface has non-trivial topologically protected surface states (SS) [3–7], which give rise to 2D Dirac fermions with an odd number of Dirac cones (1 for Bi₂Se₃) and spin-momentum locking. Most as-grown Bi₂Se₃ samples have a significant amount of (uncontrolled) Se vacancies that cause unintentional n-type bulk doping. Previous well-documented magnetotransport studies [8–10] of Bi₂Se₃ with bulk carrier densities between ~10^{17} and 10^{19} cm^{-3} show standard 3D transport behavior of a doped bulk semiconductor. Interestingly, recent measurements on Bi₂Se₃ in lower and higher carrier density regimes have both revealed novel magnetotransport behaviors. In very low bulk doping (with carrier density <10^{17} cm^{-3}) samples (synthesized with compensating dopants, such as Sb), quantum oscillations of the 2D Dirac fermions attributed to TI SS have been observed [11]. In very high bulk doping (carrier density ≳10^{19} cm^{-3}) samples, a bulk quantum Hall effect (QHE) with a 2D-like transport behavior arising from parallel QLs in the 3D bulk has been observed [12]. Here, we present comprehensive structural and electronic characterizations on such highly doped Bi₂Se₃. The structure of the crystals was analyzed by X-ray diffraction (XRD), scanning tunneling microscopy (STM), and Raman spectroscopy. The TI SS in our sample was directly revealed by angle-resolved photoemission spectroscopy (ARPES). On the other hand, our transport measurements show that the electronic conduction is dominated by the bulk. We present the temperature (T) dependent resistance data on samples with different thicknesses (from ~60 nm to 310 nm), and magnetotransport
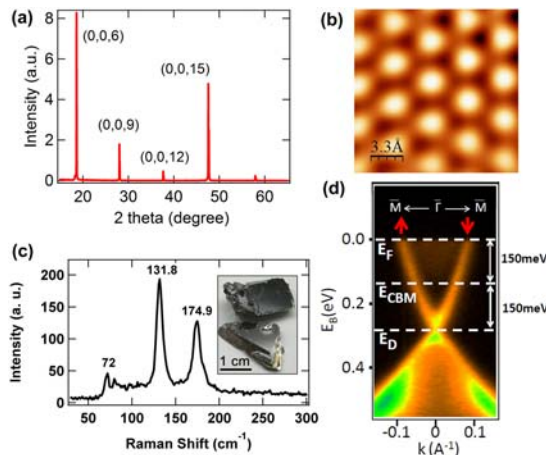
Figure 1 (online colour at: www.pss-rapid.com) (a) Representative XRD pattern on single crystal Bi$_2$Se$_3$(001) surface. The peaks are labeled with (*hkl*) Miller indices. (b) Atomic resolution STM image of a cleaved surface of Bi$_2$Se$_3$ crystal. (c) Representative Raman spectrum measured on a Bi$_2$Se$_3$ crystal. Three characteristic Raman peaks are labeled. Inset: optical image of the Bi$_2$Se$_3$ single crystals. (d) High-resolution ARPES energy-momentum dispersion band mapping along a pair of time-reversal invariant points M–Γ–M on Bi$_2$Se$_3$.

data on one of the sample ("A") confirming the previously observed bulk QHE [12] (up to higher magnetic field than that in Ref. [12]). Our results underscore the challenge of accessing surface state electronic transport (due to high bulk conduction) in as-grown Bi$_2$Se$_3$ bulk crystals. At the end of this letter, we briefly discuss several possible strategies of reducing bulk doping or conduction.

2 Results and discussion High-quality Bi$_2$Se$_3$ single crystals (optical images shown in the inset of Fig. 1c) were synthesized by the Bridgman technique (see Supporting Information, online at: www.pss-rapid.com). Figure 1a shows an XRD pattern measured on Bi$_2$Se$_3$(001) surface. The XRD reflections are attributed to Bi$_2$Se$_3$ (0,0,6) (0,0,9) (0,0,12) (0,0,15) planes, confirming the sample's single crystalline structure. From powder XRD data (not shown), we extract two lattice constants, $a = 4.137$ Å and $c = 28.679$ Å, which are consistent with the previously reported values [13, 14]. The atomic resolution STM image (Fig. 1b) of a cleaved Bi$_2$Se$_3$(001) surface was measured in ultrahigh vacuum, showing a lattice constant $a = 4.2$ Å, confirming the XRD result. The lattice structure of our samples was further investigated by Raman spectroscopy. A representative Raman spectrum is shown in Fig. 1c. Three Raman peaks at proximately 72 cm^{-1}, 131.8 cm^{-1}, and 174.9 cm^{-1} agree well with the characteristic lattice vibration modes A_{1g}^1, E_g^2 and A_{1g}^2 observed in a previous study [15]. The topological SS of our samples were directly revealed by ARPES as shown in Fig. 1d. The Fermi level is located at 150 meV above the bulk conduction band minimum (CBM) in this sample. The Fermi wave vector and Fermi velocity of the SS are found to be $k_F = 0.1$ Å^{-1} and $v_F = 5 \times 10^5$ m/s, similar to previous

APRES measurements [1] on Bi$_2$Se$_3$ (see Supporting Information for more analysis on the ARPES data).

Figure 2a shows the four-terminal longitudinal resistance (R_{xx}) of a 150 nm thick exfoliated flake (sample A) measured from room temperature down to 5 K, displaying a metallic behavior, as qualitatively expected for the highly doped bulk. The T dependence of R_{xx} can be fitted to a simplified phenomenological model developed for doped Bi$_2$Te$_3$ bulk crystals [16] (which shows generally similar transport properties as doped Bi$_2$Se$_3$):

$$R_{xx} = R_0 + \alpha \, \mathrm{e}^{-\theta/T} + \beta \, T^2 . \tag{1}$$

R_0, a low-T residual resistance, corresponds to the contributions of impurity scattering. Phonon scattering and electron−electron (e−e) scattering give rise to the exponential and the quadratic terms, respectively. We found $R_0 = 22.46$ Ω, $\alpha = 13.5$ Ω, $\theta = 217$ K and $\beta = 0.00009$ Ω/K^2 give the best fit (as shown by the red line in Fig. 2a) to the experimental data (circles in Fig. 2a). The T dependence is dominated by the phonon scattering [16] and the fitting parameter θ corresponds to an effective phonon frequency $\omega = k_B\theta/\hbar = 3.1 \times 10^{13}$ rad/s. The very small value of β indicates that the e–e scattering effect is negligible in our sample. We measured the T dependence resistivity on six samples with different thicknesses. As an indicator of the metallic behavior, we take the high-T (270 K) resistance normalized by the respective low-T (15 K) value, and plot the ratio against the sample thickness (Fig. 2b). Interestingly, the thinner samples appear to be "less metallic" as measured by this ratio. Figure 2b suggests that thinning down the crystal thickness can be an effective means to reduce the metallic bulk conduction of Bi$_2$Se$_3$ (even for samples with high bulk doping) that may help bring out the SS transport signatures that are often overwhelmed by the bulk conduction.

Figure 3a shows R_{xx} and Hall resistance R_{xy} for sample A as functions of perpendicular magnetic field (B) applied along the c-axis at 340 mK. The carrier (n-type) density and mobility extracted from the low-B measurements are 4.7×10^{19} cm^{-3} and ~400 cm^2/Vs respectively. At higher B, R_{xx} oscillates periodically in $1/B$ (with a period B_F), which can be interpreted as Shubnikov–de Haas oscillations due to the formation of Landau levels (LL). The N-th minimum of R_{xx}, counting from $B = B_F$ (which defines $N = 1$), corresponds to the N-th LL (labeled in Fig. 3a). We plot the assigned LL index N against the inverse of the magnetic field
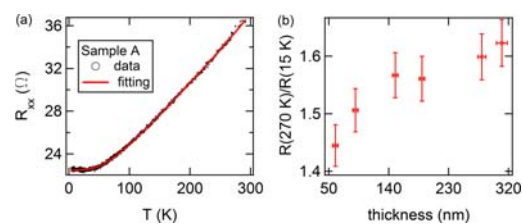

Figure 2 (online colour at: www.pss-rapid.com) (a) Temperature dependence of four-terminal longitudinal resistance (R_{xx}) in sample A. The red line shows the fitting to Eq. (1). (b) $R(T = 270$ K)/$R(T = 15$ K) plotted against sample thicknesses.
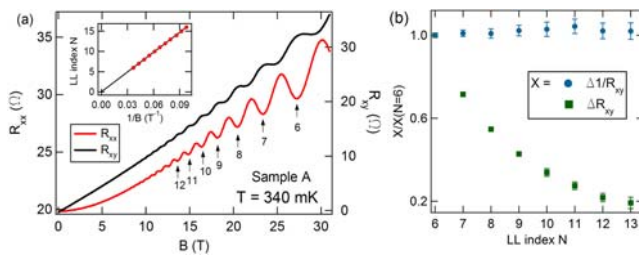
Figure 3 (online colour at: www.pss-rapid.com) (a) Hall resistance (R_{xy}) and R_{xx} of sample A as functions of magnetic field (B, perpendicular to the QLs) measured at T = 340 mK. The minima in R_{xx} corresponding to a series of Landau Level indices are labeled with arrows. Inset: LL fan diagram. (b) Normalized step size in $1/R_{xy}$ and R_{xy} plotted against LL index (N).

(B) positions of the observed minima in $R_{xx}(B)$ in the inset of Fig 3a. The black solid line is a linear fit with N-axis intercept 0 ± 0.02 and slope B_F = 163 T, corresponding to a bulk carrier Fermi wave vector $k_F = 0.07$ Å^{-1}. Furthermore, accompanying the minima in R_{xx}, R_{xy} shows developing quantized plateaus. In Fig. 3b, we plot normalized quantized Hall step size $\Delta(1/R_{xy})$ and ΔR_{xy} (difference between two adjacent plateaus in $1/R_{xy}$ and R_{xy}, respectively, then normalized by their own values at N = 6) as functions of LL index N. It clearly shows that $\Delta(1/R_{xy})$ is largely independent with increasing LL index, while ΔR_{xy} decreases. The approximately constant value of $\Delta(1/R_{xy})$ for different LLs is ~$1.2e^2/h$ per QL (the number of QLs is determined by sample's thickness, where the scaling of $\Delta(1/R_{xy})$ with the thickness as observed previously [12] further confirms that the transport is dominated by the bulk). The quantization in R_{xy} can be interpreted as a "bulk QHE" [12] attributed to parallel 2D electron gas arising from the stacking QLs in highly doped Bi_2Se_3 crystals (carrier density $\gtrsim 10^{19}$ cm^{-3}, where the Se vacancies may help reduce the electronic couplings between the QLs), and not caused by SS or any other surface conduction channels. The quantized Hall step size in $1/R_{xy}$ was examined down to lower LLs compared to our previous study [12], and confirmed to remain approximately constant for different LLs. Our results (here and in Ref. [12]), along with those from earlier experiments [10, 11, 17–19] on less-doped Bi_2Se_3, demonstrate the rich physics in the magnetotransport of Bi_2Se_3 in different regimes of bulk carrier densities.

3 Conclusion High quality Bi_2Se_3 single crystals were synthesized by Bridgman techniques. The lattice structure is characterized by XRD, STM and Raman spectroscopy that confirmed the excellent crystalline quality. Our as-grown crystals are found to have high bulk carrier density ($>10^{19}$ cm^{-3}, presumably due to substantial n-type doping by Se vacancies). The temperature dependence of resistance confirms the metallic behavior, which is weaker for thinner samples. We conducted magnetotransport measurements in a higher B field to reach lower LL compared to our previous study [12] and confirmed the bulk QHE previously observed. Accessing SS transport in as-grown Bi_2Se_3 remains challenging. There are several possible strategies to reduce the bulk conduction: for example, (i) thinning down the thickness of the crystal [20, 21]; (ii) adding more Se during growth to reduce Se vacancies (see Fig. S1 in Supporting Information); (iii) growing mixed crystals such as Bi_2Te_2Se which has been shown to have a large bulk resistivity (low bulk carrier density) [22, 23]; (iv) growing crystals with compensating dopants (e.g., Sb [11] or Ca [24]) to reduce bulk doping. Employing one or more of such strategies will likely be important to prepare TI materials for transport studies and device applications of TI SS.

References

[1] Y. Xia et al., Nature Phys. **5**, 398 (2009).
[2] H. Zhang et al., Nature Phys. **5**, 438 (2009).
[3] X.-L. Qi and S.-C. Zhang, Phys. Today **63**, 33 (2010).
[4] M. Z. Hasan and J. E. Moore, Annu. Rev. Condens. Matter **2**, 55 (2011).
[5] M. Hasan and C. Kane, Rev. Mod. Phys. **82**, 3045 (2010).
[6] J. E. Moore, Nature **464**, 194 (2010).
[7] H. C. Manoharan, Nature Nanotechnol. **5**, 477 (2010).
[8] H. Köhler, Physica Status Solidi B **58**, 91 (1973).
[9] V. A. Kulbachinskii et al., Phys. Rev. B **59**, 15733 (1999).
[10] J. G. Analytis et al., Phys. Rev. B **81**, 205407 (2010).
[11] J. G. Analytis et al., Nature Phys. **6**, 960 (2010).
[12] H. Cao et al., Phys. Rev. Lett. **108**, 216803 (2012).
[13] R. W. G. Wyckoff, Crystal Structures (John Wiley & Sons, New York, London, 1964).
[14] X. Chen et al., Appl. Phys. Lett. **99**, 261912 (2011).
[15] W. Richter et al., Phys. Status Solidi B **84**, 619 (1977).
[16] W. T. Pawlewicz et al., Phys. Lett. A **48**, 391 (1974).
[17] H. Köhler and H. Fischer, Phys. Status Solidi B **69**, 349 (1975).
[18] V.A. Kulbachinskii et al., J. Phys. Soc. Jpn. **68**, 3328 (1999).
[19] N. P. Butch et al., Phys. Rev. B **81**, 241301 (2010).
[20] H. Steinberg et al., Nano Lett. **10**, 5032 (2010).
[21] F. Qu et al., J. Low Temp. Phys., online first (2012).
[22] Z. Ren et al., Phys. Rev. B **82**, 241306 (2010).
[23] J. Xiong et al., Physica E **44**, 917 (2012).
[24] D. Hsieh et al., Nature **460**, 1101 (2009).